Monthly Notices of the ROYAL ASTRONOMICAL SOCIETY

MNRAS **473,** 4538–4543 (2018) doi:10.1093/mnras/stx2572
Advance Access publication 2017 October 3

Where does galactic dust come from?

M. Ginolfi,[1]★ L. Graziani,[1] R. Schneider,[1,2] S. Marassi,[1] R. Valiante,[1] F. Dell'Agli,[3,4] P. Ventura[1] and L. K. Hunt[5]

[1]*INAF - Osservatorio Astronomico di Roma, via Frascati 33, I-00078 Monte Porzio Catone, Roma, Italy*
[2]*Dipartimento di Fisica, 'Sapienza' Università di Roma, Piazzale Aldo Moro 5, I-00185, Roma, Italy*
[3]*Instituto de Astrofisica de Canarias, Via Lactea, E-38205 La Laguna, Tenerife, Spain*
[4]*Departamento de Astrofisica, Universidad de La Laguna (ULL), E-38206 La Laguna, Spain*
[5]*INAF/Osservatorio Astrofisico di Arcetri, Largo E. Femi 5, I-50125 Firenze, Italy*

Accepted 2017 September 29. Received 2017 September 27; in original form 2017 July 17

ABSTRACT

Here we investigate the origin of the dust mass ($M_{\rm dust}$) observed in the Milky Way (MW) and of dust scaling relations found in a sample of local galaxies from the DGS and KINGFISH surveys. To this aim, we model dust production from Asymptotic Giant Branch (AGB) stars and supernovae (SNe) in simulated galaxies forming along the assembly of a MW-like halo in a well-resolved cosmic volume of 4 cMpc using the GAMESH pipeline. We explore the impact of different sets of metallicity and mass-dependent AGB and SN dust yields on the predicted $M_{\rm dust}$. Our results show that models accounting for grain destruction by the SN reverse shock predict a total dust mass in the MW, that is a factor of ∼4 less than observed, and cannot reproduce the observed galaxy-scale relations between dust and stellar masses, and dust-to-gas ratios and metallicity, with a smaller discrepancy in galaxies with low metallicity ($12 + \log({\rm O/H}) < 7.5$) and low stellar masses ($M_{\rm star} < 10^7\,{\rm M}_\odot$). In agreement with previous studies, we suggest that competing processes in the interstellar medium must be at play to explain the observed trends. Our result reinforces this conclusion by showing that it holds independently of the adopted AGB and SN dust yields.

Key words: stars: AGB and post-AGB – supernovae: general – dust, extinction – local interstellar matter – galaxies: evolution.

1 INTRODUCTION

Interstellar dust plays a major role in driving galaxy evolution along cosmic time due to its tight connection with both star formation (SF) and the thermal and chemical evolution of the interstellar medium (ISM). Dust grains can shield molecules from the photodissociating radiation and trigger the formation of molecular hydrogen (H_2), acting as an efficient catalyst of atomic hydrogen (HI) reactions. In addition, dust shapes the observed galaxy colours by absorbing and scattering stellar light at ultraviolet (UV) and visible wavelengths, and re-emitting infrared (IR) radiation.

Interstellar dust grains are produced in the circumstellar envelopes of asymptotic giant branch (AGB) stars (Ferrarotti & Gail 2006; Zhukovska, Gail & Trieloff 2008; Ventura et al. 2012a,b; Di Criscienzo et al. 2013; Nanni et al. 2013; Ventura et al. 2014; Dell'Agli et al. 2015, 2017) and in the ejecta of core-collapse supernovae (SNe, Todini & Ferrara 2001; Schneider, Ferrara & Salvaterra 2004; Bianchi & Schneider 2007; Nozawa et al. 2007; Cherchneff & Dwek 2009, 2010; Sarangi & Cherchneff 2013, 2015; Marassi et al. 2014, 2015; Bocchio et al. 2016; Sluder, Milosavljevic & Montgomery 2016).

Once created by stellar sources and injected into the ISM, these grains could evolve by physical processes capable of destroying or growing them. The key mechanisms responsible for dust destruction are collisions between grains, SN shocks and thermal sputtering (Draine & Salpeter 1979; McKee et al. 1987; Jones, Tielens & Hollenbach 1996, Hirashita 2010; Jones & Nuth 2011; Bocchio, Jones & Slavin 2014). Grains may also grow by accretion of gas-phase metals within dense molecular clouds (Draine 1990; Dominik & Tielens 1997; Inoue 2011; Hirashita 2012; Köhler, Ysard & Jones 2015), thus increasing the dust mass.

Although the efficiency or even the physical nature of these processes is still highly debated (Ferrara, Viti & Ceccarelli 2016, but also see Zhukovska et al. 2016), grain growth has been often invoked by galactic chemical evolution models as the dominant process responsible for production of the dust mass inferred from observations of local (de Bennassuti et al. 2014; Zhukovska 2014; McKinnon,

★ E-mail: michele.ginolfi@oa-roma.inf.it

Torrey & Vogelsberger 2016; Schneider, Hunt & Valiante 2016; Gioannini, Matteucci & Calura 2017; Popping, Somerville & Galametz 2017) and high-redshift galaxies (Rowlands et al. 2014; Mancini et al. 2015, 2016; Michałowski 2015; Watson et al. 2015; Aoyama et al. 2017; Knudsen et al. 2017; Wang, Hirashita & Hou 2017). Moreover strong indications for grain growth acting in the ISM come from sub-millimetre (submm) observations of high redshift quasar host galaxies (Mattsson 2011; Pipino et al. 2011; Valiante et al. 2011; Calura et al. 2014; Valiante et al. 2014) and gamma-ray burst damped Lyman-alpha absorbers (Wiseman et al. 2017). Finally, only chemical evolution models accounting for dust growth in the ISM (e.g. Asano et al. 2013; de Bennassuti et al. 2014; Zhukovska 2014; Popping et al. 2017) can successfully reproduce the observed trend between dust-to-gas mass ratio (D/G) and metallicity (Rémy-Ruyer et al. 2014, 2015), or can explain the gas surface density dependence of D/G observed in the Magellanic Clouds by *IRAS* and *Planck* (Roman-Duval et al. 2017).

In this paper we investigate the efficiency of stellar mechanisms of dust production, aiming at interpreting the dust mass budget of the Milky Way (MW) and the relations between the dust mass ($M_{\rm dust}$), stellar mass ($M_\star$), D/G and metallicity (Z) observed for a wide sample of galaxies, spanning ∼2 dex in Z and ∼5 dex in $M_\star$ (see Section 2).

For this reason, we have implemented different models of dust formation from stellar sources (e.g. Ferrarotti & Gail 2006; Bianchi & Schneider 2007; Zhukovska et al. 2008; Dell'Agli et al. 2015, 2017; Marassi et al. 2015; Bocchio et al. 2016) in the latest release of the GAMESH pipeline (Graziani et al. 2015), capable of reproducing the stellar, gas and metal mass observed in the MW as well as the fundamental scaling relations in the redshift range $0 < z < 4$ (Graziani et al. 2017).

The paper is organized as follows. In Section 2, we briefly describe the sample of data used for the comparisons with our results. In Section 3, we summarize the properties of the GAMESH pipeline, and we describe the adopted stellar yields of dust production and their modelling. Sections 4 and 5 show the results of this work and a discussion of their astrophysical implications.

2 SAMPLE AND OBSERVATIONS

Two samples of local galaxies observed with *Herschel* have been used for comparison with our models: the Dwarf Galaxy Survey (DGS, Madden et al. 2013) and the Key Insights on Nearby Galaxies: a Far-Infrared Survey with *Herschel* (KINGFISH, Kennicutt et al. 2011). These samples are extensively described in Rémy-Ruyer et al. (2014, 2015). The DGS is a sample of 48 star-forming dwarf galaxies with low metallicity ranging from $12 + \log({\rm O/H}) = 7.14$ to 8.43. Stellar masses span ∼4 dex, from 3×10^6 to $\sim 3 \times 10^{10}\,{\rm M}_\odot$. The KINGFISH sample contains 61 galaxies with metallicity in the range $12 + \log({\rm O/H}) = 7.54$–$8.77$ and stellar masses in the range $[2 \times 10^7$–$1.4 \times 10^{11}]{\rm M}_\odot$, and it probes more metal-rich and massive environments. The metallicities of the DGS galaxies have been derived using empirical strong emission-line methods (Madden et al. 2013), and DGS dust masses have been computed by Rémy-Ruyer et al. (2015). DGS stellar masses were taken from Madden et al. (2014), who used the prescription of Eskew, Zaritsky & Meidt (2012) and the IRAC 3.6 μm and 4.5 μm luminosities. KINGFISH metallicities have been taken from Hunt et al. (2016), recalibrated to the Pettini & Pagel (2004) strong-line N2 calibration, and dust masses taken from Hunt et al. (in preparation) using the photometry presented by Dale et al. (2017). Stellar masses for KINGFISH are taken from Hunt et al. (2016), computed from the IRAC 3.6 μm luminosities according to Wen et al. (2013). Gas masses for both the DGS and the KINGFISH samples are obtained by combining the contribution of HI (see Draine et al. 2007 for the KINGFISH galaxies and Madden et al. 2013 for DGS) and molecular gas, derived through CO measurements (Rémy-Ruyer et al. 2015).

To compare our predictions with the dust mass budget of the MW, observed values from Planck Collaboration XXV (2011) and Bovy & Rix (2013) (where the measured gas mass is converted into dust mass using a standard $(D/G)_{\rm MW} \sim 1/100$; Draine et al. 2007) have been adopted.

3 MODEL DESCRIPTION

The cosmological simulation has been performed with the latest release of the GAMESH pipeline (Graziani et al. 2015, 2017) which combines a high-resolution N-body simulation,[1] a novel version of the semi-analytic, data-constrained model GAMETE (Salvadori, Schneider & Ferrara 2007) and the third release of the radiative transfer code CRASH (Graziani, Maselli & Ciardi 2013) computing gas ionization through hydrogen, helium and metals.

GAMESH follows the cosmological evolution of a cubic volume of 4 cMpc side length, centred on a well-resolved MW-like halo,[2] by accounting for star formation, chemical enrichment, Pop III/Pop II transition and SN-driven feedback. Comparison with recent observations of candidate MW progenitors at $0 < z < 2.5$ reproduce the galaxy main sequence, the mass–metallicity relation and the Fundamental Plane of metallicity relations at $0 < z < 4$ (Graziani et al. 2017). The interested reader can find more details in Graziani et al. (2015, 2017) and Schneider et al. (2017).

The present work adopts a novel extension of GAMESH in which dust formation by stellar sources is computed, moving its semi-analytic scheme towards more advanced release of GAMETE (Valiante et al. 2014; de Bennassuti et al. 2017). For the purpose of this study, we neglect dust destruction by interstellar shocks and the only physical mechanism that can decrease the dust content of the ISM is astration. To maintain the flexibility of the GAMESH pipeline, the current release runs on different theoretical models of stellar dust yields, which we briefly describe below.

3.1 Modelling dust production yields

AGB and SNe have been considered as the two major dust producers. Their relative importance depends on the stellar initial mass function (IMF), on the star formation history and on the mass and metallicity dependence of the stellar dust yields (Valiante et al. 2009). Using AGB dust yields from Ferrarotti & Gail (2006) and Zhukovska et al. (2008, hereafter Z08) and SN dust yields from Bianchi & Schneider (2007, hereafter BS07), Valiante et al. (2009) showed that AGB stars can contribute and eventually dominate dust enrichment on relatively short evolutionary time-scales (150–200 Myr) when the stars are assumed to form in a burst with a Salpeter-like IMF. Recently, a new grid of AGB dust yields for stars with masses in the range $[1 - 8]\,{\rm M}_\odot$ and metallicity $0.01\,{\rm Z}_\odot \leq Z \leq {\rm Z}_\odot$ has been computed by Ventura et al. (2012a,b, 2014),

[1] The N-body simulation is based on the code GCD+ (Kawata et al. 2013) and adopts a flat ΛCDM cosmology with $\Omega_{\rm m} = 0.32$, $\Omega_\Lambda = 0.68$, $\Omega_{\rm b} = 0.049$ and $h = 0.67$ (Planck Collaboration XVI 2014).

[2] The MW-like halo has a mass $M_{\rm MW} = 1.7 \times 10^{12}\,{\rm M}_\odot$ at $z = 0$ and it is resolved with a dark matter particle resolution mass of $3.4 \times 10^5\,{\rm M}_\odot$.

Di Criscienzo et al. (2013) and Dell'Agli et al. (2017). These are based on numerically integrated stellar models by means of the ATON code and predict a different mass and metallicity dependence of dust production rates with respect to Z08.[3] As a result, assuming the stars to form in a single burst with a Salpeter-like IMF and adopting these new AGB dust yields (hereafter ATON yields), Schneider et al. (2015) has found that when the initial metallicity of the stars is $Z \leq 0.2\,Z_{\odot}$, the contribution of AGB stars is always sub-dominant with respect to that of SNe and dominate on a time-scale ∼500 Myr only at higher metallicity.

The above conclusion depends on the adopted SN yields and on the fraction of freshly formed dust that gets destroyed by the passage of the SN reverse shock generated by the interaction of the SN blast wave with its surrounding medium and propagating through the ejecta. This shock triggers the destruction of SN-condensed dust grains through thermal sputtering due to the interaction of dust grains with particles in the gas, sublimation due to collisional heating to high temperatures, and vaporization of part of the colliding grains during grain–grain collisions (Bianchi & Schneider 2007; Nozawa et al. 2007; Silvia, Smith & Shull 2010, 2012; Marassi et al. 2014, 2015; Bocchio et al. 2016; Micelotta, Dwek & Slavin 2016). Here we explore different combinations of SN dust yields and reverse shock destruction efficiencies. We consider the metallicity- and mass-dependent SN dust yields computed by BS07 applying standard nucleation theory to the grid of SN explosion models by Woosley & Weaver (1995) with progenitor masses in the range $[12–40]\,M_{\odot}$, metallicity $[10^{-4}-1]\,Z_{\odot}$ and adopting a constant explosion energy of 1.2×10^{51} ergs. When no reverse shock is considered, the predicted SN dust yields are in the range $[0.1–0.6]\,M_{\odot}$. We also consider the effects of reverse shock destruction, adopting the model where the circumstellar medium density is $\sim 1\,\mathrm{cm}^{-3}$, which leads to ≈10 per cent smaller dust yields. When compared to *Herschel* data of young SN remnants, these two sets of yields appear to bracket the inferred dust masses (Schneider et al. 2015).

For this study we also adopt new SN dust yields spanning a larger range of progenitor masses and metallicity (Marassi et al., in preparation). In particular, we consider the grid of *calibrated* SN models, where the explosion energy is not fixed a priori (Limongi 2017) but is instead calibrated requiring the ejection of a specific amount of radioactive ^{56}Ni for each SN progenitor. The amount of ^{56}Ni for each SN progenitor is obtained from the best fit of the observations (Marassi et al., in preparation). For these SN dust yields, we assume that in the range [1–8] per cent of the original dust mass is able to survive the passage of the reverse shock, contributing to dust enrichment. These values have been calibrated on the results obtained by Bocchio et al. (2016), where the new code GRASH-Rev[4] has been applied to four SN models selected to best fit the properties of SN 1987A, CasA, the Crab nebula and N49, which have been observed with both *Spitzer* and *Herschel*. This study (e.g. Bocchio et al. 2016) suggests that the largest dust mass destruction is predicted to occur between 10^3 and 10^5 yr after the explosion. As a result, since the oldest SN in the sample has an age of 4800 yr, the observed dust mass can only provide an upper limit to the mass of SN dust that will enrich the ISM.

[3] We refer to the original papers for a thorough discussion of the models and a comparison with Z08 models.

[4] GRASH-Rev follows the dynamics of dust grains in the shocked SN ejecta and computes the time evolution of the mass, composition and size distribution of the grains (Bocchio et al. 2016).

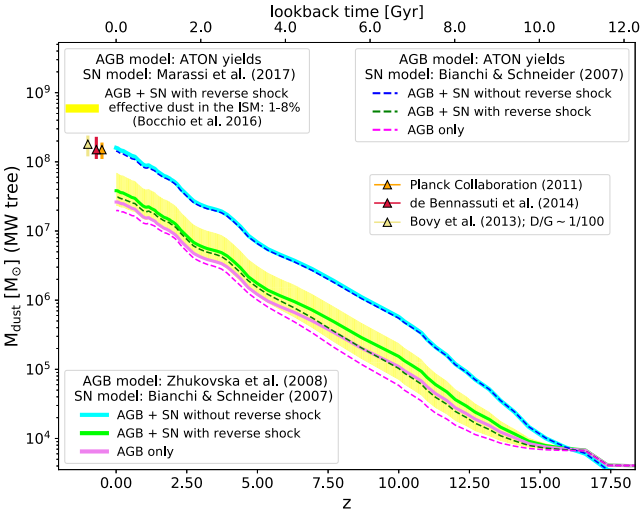

Figure 1. The dust mass evolution of the MW-sized halo as a function of redshift and lookback time. Different line styles correspond to different models of dust production by stellar sources: solid lines (dashed lines) refer to SN dust yields by BS07 and AGB dust yields by Z08 (ATON). Different line colours discriminate RS and nRS models (see the legends). An AGB-only model is also explored (pink lines). The shaded yellow region corresponds to the new M17 (SN) + ATON (AGB) model. The triangular points represent the MW dust mass at $z = 0$, as inferred by observations from Planck Collaboration XXV (2011) (orange) and Bovy & Rix (2013) (yellow, in this case the measured gas mass has been converted in dust mass assuming a standard $D/G_{\mathrm{MW}} \sim 1/100$) and simulations (de Bennassuti et al. 2014).

4 RESULTS

Here we show the results of simulations where we adopt different combinations of dust production models by stellar sources. When considering SN contributions, we discuss separately the two cases with (RS) and without (nRS) the effects of the reverse shock. In Section 4.1 we compare the observed dust mass of the MW with masses arising from different models of dust production in our simulations. In Section 4.2 we extend the comparison to a distribution of local galaxies spanning a wide range in metallicities and stellar masses.

4.1 MW dust mass assembly

The dust mass assembly in the MW-sized halo is shown in Fig. 1 as a function of redshift and lookback time. Pink (solid/dashed) lines refer to the amount of dust produced by AGB stars only: it is immediately evident that, independently of the adopted yields, these stars alone cannot produce more than $\sim 3 \times 10^7\,M_{\odot}$ of dust, with a discrepancy of ∼30 per cent between old (Z08) and new (ATON) models. The higher dependence on metallicity of ATON yields leads to lower dust masses at $z \gtrsim 5$. At all redshifts, SNe dominate dust production, even in the RS case. The comparison of model predictions with observations shows that the existing dust mass ($M_{\mathrm{dust}} \sim 1.5 \times 10^8\,M_{\odot}$) in the MW can be produced by stellar dust sources only if all the dust formed in AGB and SN ejecta is injected in the ISM without suffering destruction by the RS (cyan and blue dashed lines). We consider this to be an unrealistic assumption. In fact, Bocchio et al. (2016) show that while SN 1987A is too young for the reverse shock to have affected the dust mass, in Cas A, Crab and N49 the reverse shock has already destroyed between 10 and 40 per cent of the initial dust mass, despite the relatively young age of these SN remnants.

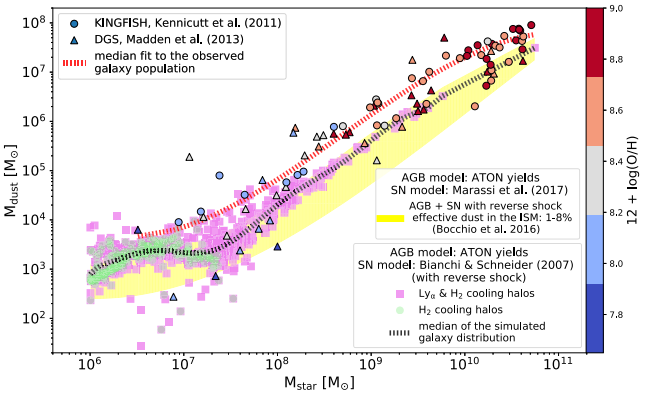

Figure 2. The dust mass of simulated galaxies (pink squares) at $z = 0$ as a function of their stellar mass. Green dots represent the sub-sample of galaxies with virial temperature $T_{vir} < 2 \times 10^4$ K. The black dashed line indicates the median trend of the simulated galaxy distribution. Here, ATON + BS07 (with RS) and ATON + M17 (with RS) models for dust production by stellar sources are adopted. Observational points of galaxies from the DGS (triangles) and KINGFISH (circles) surveys are shown, colour coded for different values of their metallicity. The red dashed line indicates the median trend of the observed galaxy distribution.

On the other hand, when the reverse shock effect is included, the dust mass produced by stellar sources and effectively injected into the ISM (i.e. the grains which survive the passage of the shock) is a factor ∼4 lower than the observed value, as shown by Fig. 1. Here the yellow area shows the M17 with RS models (with the upper and lower boundaries corresponding to 1–8 per cent destruction), in good agreement with predictions from the old stellar yields of BS07 with RS.

We conclude that, independent of the dust production yields, a model where dust has only a stellar origin fails at reproducing the total dust mass in the MW. As other metallicity-related relations are correctly predicted by the simulation (Graziani et al. 2017), we interpret this result as a clear indication that dust evolution in the MW ISM plays an important role. Moreover, as both dust destruction (likely acting in the hot ISM phase) and grain growth in the cold ISM are missing in the present model, Fig. 1 suggests an efficient process of dust growth, capable of compensating both the missing factor ∼4 commented above, and the additional effects of dust sputtering and destruction acting in the hot medium of the MW halo.

4.2 Dust abundances in galaxies at $z \sim 0$

Here we extend our analysis by comparing in Fig. 2 the M_{dust}–$M_\star$ relation of simulated galaxies at $z = 0$ with local observations from the DGS and KINGFISH surveys (see Section 2). Hereafter we adopt the ATON yields for AGB stars and SN yields by the BS07 and by MR17 with RS. The symbols indicating the observed galaxies are colour coded (see colour palette in the figure) for different values of their metallicity. Fig. 2 shows that the dust masses predicted by the simulation are (on average) systematically lower (a factor ∼3) than the observed ones, at any given stellar mass. Such a discrepancy decreases towards the low-$M_\star$ tail of the distribution, where observed galaxies are mostly metal poor ($12 + \log(O/H) \lesssim 8$). This result confirms – on a statistical sample of local galaxies – that dust produced by stellar sources alone is insufficient to account for the observed mass. Depending on the efficiency of the reverse shock

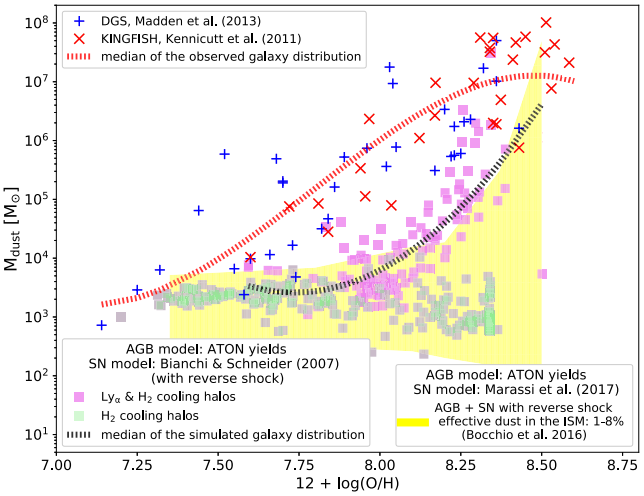

Figure 3. Dust mass as a function of metallicity. Lines and symbols are the same as in Fig. 2 but observations from the DGS and KINGFISH surveys are shown as blue plus and red crosses. The black dashed line indicates the median trend of the observed galaxy distribution.

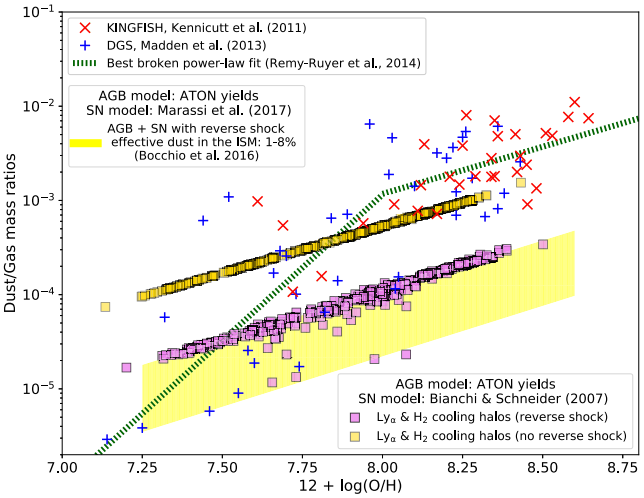

Figure 4. The D/G of simulated galaxies at $z \sim 0$ as a function of their metallicity. Lines and symbols are the same as in Fig. 3. For comparison, we also show the ATON + BS07 model with nRS (yellow squares) and the broken power-law fit to the observed galaxy distribution computed in Rémy-Ruyer et al. (2014) (green dashed line).

model, the new SN models seem to largely underpredict the observed trends (see yellow area), shifting the predicted median at lower dust masses, at fixed $M_\star$.

Similar considerations arise from Fig. 3 where we show the M_{dust}–Z relation. The observed dust mass–metallicity relation is largely underpredicted by the simulations, both for galaxies hosted in Lyα-cooling and in H_2-cooling haloes. In addition, the comparison of the two dashed lines shows that the simulated galaxies fail to reproduce the observed average trend.

Finally Fig. 4 shows the D/G of simulated galaxies at $z \sim 0$ as a function of their metallicity. Observational data from the DGS and KINGFISH surveys are reported, and the brokenpower-law fit to the D/G–Z relation, computed by Rémy-Ruyer et al. (2014), is also shown as the dashed line. In addition to the reference models considered in the previous figures, here we also show the ATON + BS07 model with nRS (yellow squares). In models where the SN

dust yields are reduced by the effect of the RS, the D/G of the simulated galaxies confirm our previous conclusions, being about one order of magnitude lower than the observed one at intermediate–high metallicity. Such a discrepancy tends to decrease in the low-Z tail of the galaxy distribution ($12 + \log(\mathrm{O/H}) \lesssim 8$), where the observed D/G–Z enters a new regime (i.e. the slope changes). When nRS is considered, the predicted D/G of simulated galaxies at high metallicity are closer to the observed values. However, regardless of the adopted stellar yields, none of the models is able to reproduce the observed double power-law trend of the D/G–Z relation (Hirashita 2012; Asano et al. 2013; Zhukovska 2014).

5 DISCUSSION AND CONCLUSIONS

Our results confirm that dust evolution models accounting for 'stellar production-only' fail at reproducing a number of observables. In particular:

(i) the dust mass produced by stars in the MW and effectively injected into the ISM after surviving the passage of the SN reverse shock is predicted to be a factor ∼4 lower than observed, with the uncertainty depending on which model of dust formation by AGB stars is adopted (see Fig. 1).

(ii) the predicted dust mass budget of the simulated population of local galaxies results to be, on average, systematically underestimated with respect to observations, with visible consequences arising when comparing our simulated $M_{\rm dust}$–$M_\star$ (Fig. 2), $M_{\rm dust}$–Z (Fig. 3) and D/G–Z (Fig. 4) relations with the observed trends. Nevertheless, there are insights about such a discrepancy declining in proximity of the low-Z and low-$M_\star$ tails of the galaxy distribution.

Hence the amount of dust injected into the ISM by SN explosions (accounting for the destructive effect of the reverse shock) and AGB stellar winds is not sufficient to reproduce the observed mass of interstellar dust. The inclusion of dust destruction by interstellar shocks, that we have neglected, would further strengthen this conclusion.

For completeness, we tested the hypothesis that dust grains formed in SN ejecta are injected in the ISM without being affected by the passage of the reverse shock. While this unrealistic model succeeds at reproducing the observed dust mass of the MW (Fig. 1), it fails at reproducing the observed D/G–Z relation in the low-Z tail of the local galaxy population.

Altogether our results suggest that additional (non-stellar) mechanisms of dust growth are at play during the galaxy evolution across cosmic times. Our findings are consistent with a number of previous works (see Section 1) where a significant grain growth in the dense phase of the ISM has been invoked as a supplementary process to explain the rapid dust enrichment observed in high-Z objects (Valiante et al. 2011, 2014; Mattsson 2011; Pipino et al. 2011; Calura et al. 2014; Mancini et al. 2015, 2016; Michałowski 2015), as well as the observed D/G–Z trend in local galaxies (de Bennassuti et al. 2014; Rémy-Ruyer et al. 2014; Zhukovska 2014; Schneider et al. 2016; Popping et al. 2017) and the strong gas density dependence of the D/G observed in the Magellanic Clouds (Roman-Duval et al. 2017). Our work strengthens these previous findings by showing that these conclusions are largely independent of the adopted dust yields and reverse shock modelling.

A natural consequence of these results is that data-calibrated models of the ISM in galaxy evolution must consider additional channels responsible for both dust formation in the dense phase and dust destruction in the hot phase. A deeper understanding of these phenomena is deferred to future works, where an improved version of the GAMESH pipeline, providing for an accurate modelling of the multiphase ISM, will be exploited.

ACKNOWLEDGEMENTS

The research leading to these results has received funding from the European Research Council under the European Union's Seventh Framework Programme (FP/2007- 2013)/ERC Grant Agreement n. 306476. FD acknowledges support provided by the MINECO grant AYA-2014-58082-P.

REFERENCES

Aoyama S., Hou K.-C., Shimizu I., Hirashita H., Todoroki K., Choi J.-H., Nagamine K., 2017, MNRAS, 466, 105
Asano R. S., Takeuchi T. T., Hirashita H., Inoue A. K., 2013, Earth, Planets and Space, 65, 213
Bianchi S., Schneider R., 2007, MNRAS, 378, 973
Bocchio M., Jones A. P., Slavin J. D., 2014, A&A, 570, A32
Bocchio M., Marassi S., Schneider R., Bianchi S., Limongi M., Chieffi A., 2016, A&A, 587, A157
Bovy J., Rix H.-W., 2013, ApJ, 779, 115
Calura F., Gilli R., Vignali C., Pozzi F., Pipino A., Matteucci F., 2014, MNRAS, 438, 2765
Cherchneff I., Dwek E., 2009, ApJ, 703, 642
Cherchneff I., Dwek E., 2010, ApJ, 713, 1
Dale D. A. et al., 2017, ApJ, 837, 90
de Bennassuti M., Schneider R., Valiante R., Salvadori S., 2014, MNRAS, 445, 3039
de Bennassuti M., Salvadori S., Schneider R., Valiante R., Omukai K., 2017, MNRAS, 465, 926
Dell'Agli F., Ventura P., Schneider R., Di Criscienzo M., García-Hernández D. A., Rossi C., Brocato E., 2015, MNRAS, 447, 2992
Dell'Agli F., García-Hernández D. A., Schneider R., Ventura P., La Franca F., Valiante R., Marini E., Di Criscienzo M., 2017, MNRAS, 467, 4431
Di Criscienzo M. et al., 2013, MNRAS, 433, 313
Dominik C., Tielens A. G. G. M., 1997, ApJ, 480, 647
Draine B. T., 1990, in Blitz L., ed., ASP Conf. Ser. Vol. 12, The Evolution of the Interstellar Medium. Astron. Soc. Pac., San Francisco, p. 193
Draine B. T., Salpeter E. E., 1979, ApJ, 231, 77
Draine B. T. et al., 2007, ApJ, 663, 866
Eskew M., Zaritsky D., Meidt S., 2012, AJ, 143, 139
Ferrara A., Viti S., Ceccarelli C., 2016, MNRAS, 463, L112
Ferrarotti A. S., Gail H.-P., 2006, A&A, 447, 553
Gioannini L., Matteucci F., Calura F., 2017, MNRAS, 471, 4615
Graziani L., Maselli A., Ciardi B., 2013, MNRAS, 431, 722
Graziani L., Salvadori S., Schneider R., Kawata D., de Bennassuti M., Maselli A., 2015, MNRAS, 449, 3137
Graziani L., de Bennassuti M., Schneider R., Kawata D., Salvadori S., 2017, MNRAS, 469, 1101
Hirashita H., 2010, MNRAS, 407, L49
Hirashita H., 2012, MNRAS, 422, 1263
Hunt L., Dayal P., Magrini L., Ferrara A., 2016, MNRAS, 463, 2002
Inoue A. K., 2011, Earth, Planets and Space, 63, 1027
Jones A. P., Nuth J. A., 2011, A&A, 530, A44
Jones A. P., Tielens A. G. G. M., Hollenbach D. J., 1996, ApJ, 469, 740
Kawata D., Okamoto T., Gibson B. K., Barnes D. J., Cen R., 2013, MNRAS, 428, 1968
Kennicutt R. C. et al., 2011, PASP, 123, 1347
Knudsen K. K., Watson D., Frayer D., Christensen L., Gallazzi A., Michałowski M. J., Richard J., Zavala J., 2017, MNRAS, 466, 138
Köhler M., Ysard N., Jones A. P., 2015, A&A, 579, A15
Limongi M., 2017, preprint (arXiv:1706.01913)
McKee C. F., Hollenbach D. J., Seab G. C., Tielens A. G. G. M., 1987, ApJ, 318, 674
McKinnon R., Torrey P., Vogelsberger M., 2016, MNRAS, 457, 3775

Madden S. C. et al., 2013, PASP, 125, 600
Madden S. C. et al., 2014, PASP, 126, 1079
Mancini M., Schneider R., Graziani L., Valiante R., Dayal P., Maio U., Ciardi B., Hunt L. K., 2015, MNRAS, 451, L70
Mancini M., Schneider R., Graziani L., Valiante R., Dayal P., Maio U., Ciardi B., 2016, MNRAS, 462, 3130
Marassi S., Chiaki G., Schneider R., Limongi M., Omukai K., Nozawa T., Chieffi A., Yoshida N., 2014, ApJ, 794, 100
Marassi S., Schneider R., Limongi M., Chieffi A., Bocchio M., Bianchi S., 2015, MNRAS, 454, 4250
Mattsson L., 2011, MNRAS, 414, 781
Micelotta E. R., Dwek E., Slavin J. D., 2016, A&A, 590, A65
Michałowski M. J., 2015, A&A, 577, A80
Nanni A., Bressan A., Marigo P., Girardi L., 2013, MNRAS, 434, 2390
Nozawa T., Kozasa T., Habe A., Dwek E., Umeda H., Tominaga N., Maeda K., Nomoto K., 2007, ApJ, 666, 955
Pettini M., Pagel B. E. J., 2004, MNRAS, 348, L59
Pipino A., Fan X. L., Matteucci F., Calura F., Silva L., Granato G., Maiolino R., 2011, A&A, 525, A61
Planck Collaboration XXV, 2011, A&A, 536, A25
Planck Collaboration XVI, 2014, A&A, 571, A16
Popping G., Somerville R. S., Galametz M., 2017, MNRAS, 471, 3152
Rémy-Ruyer A. et al., 2014, A&A, 563, A31
Rémy-Ruyer A. et al., 2015, A&A, 582, A121
Roman-Duval J., Bot C., Chastenet J., Gordon K., 2017, ApJ, 841, 19
Rowlands K., Gomez H. L., Dunne L., Aragón-Salamanca A., Dye S., Maddox S., da Cunha E., van der Werf P., 2014, MNRAS, 441, 1040
Salvadori S., Schneider R., Ferrara A., 2007, MNRAS, 381, 647
Sarangi A., Cherchneff I., 2013, ApJ, 776, 107
Sarangi A., Cherchneff I., 2015, A&A, 575, A95
Schneider R., Ferrara A., Salvaterra R., 2004, MNRAS, 351, 1379
Schneider R., Valiante R., Ventura P., dell'Agli F., di Criscienzo M., 2015, in Kerschbaum F., Wing R. F., Hron J., eds, ASP Conf. Ser. Vol. 497, Why Galaxies Care about AGB Stars III: A Closer Look in Space and Time. Astron. Soc. Pac., San Francisco, p. 369
Schneider R., Hunt L., Valiante R., 2016, MNRAS, 457, 1842
Schneider R., Graziani L., Marassi S., Spera M., Mapelli M., Alparone M., de Bennassuti M., 2017, MNRAS, 471, L105
Silvia D. W., Smith B. D., Shull J. M., 2010, ApJ, 715, 1575
Silvia D. W., Smith B. D., Shull J. M., 2012, ApJ, 748, 12
Sluder A., Milosavljevic M., Montgomery M. H., 2016, preprint (arXiv: 1612.09013)
Todini P., Ferrara A., 2001, MNRAS, 325, 726
Valiante R., Schneider R., Bianchi S., Andersen A. C., 2009, MNRAS, 397, 1661
Valiante R., Schneider R., Salvadori S., Bianchi S., 2011, MNRAS, 416, 1916
Valiante R., Schneider R., Salvadori S., Gallerani S., 2014, MNRAS, 444, 2442
Ventura P. et al., 2012a, MNRAS, 420, 1442
Ventura P. et al., 2012b, MNRAS, 424, 2345
Ventura P., Dell'Agli F., Schneider R., Di Criscienzo M., Rossi C., La Franca F., Gallerani S., Valiante R., 2014, MNRAS, 439, 977
Wang W.-C., Hirashita H., Hou K.-C., 2017, MNRAS, 465, 3475
Watson D., Christensen L., Knudsen K. K., Richard J., Gallazzi A., Michałowski M. J., 2015, Nature, 519, 327
Wen X.-Q., Wu H., Zhu Y.-N., Lam M. I., Wu C.-J., Wicker J., Zhao Y.-H., 2013, MNRAS, 433, 2946
Wiseman P., Schady P., Bolmer J., Krühler T., Yates R. M., Greiner J., Fynbo J. P. U., 2017, A&A, 599, A24
Woosley S. E., Weaver T. A., 1995, ApJS, 101, 181
Zhukovska S., 2014, A&A, 562, A76
Zhukovska S., Gail H.-P., Trieloff M., 2008, A&A, 479, 453
Zhukovska S., Dobbs C., Jenkins E. B., Klessen R. S., 2016, ApJ, 831, 147

This paper has been typeset from a TEX/LATEX file prepared by the author.